RABBIT: A Rapid Low Fidelity BVI Prediction Tool — Comparison and Validation using the NASA RVLT Toolchain

Lauren Weist
Aerospace Engineer
Aeromechanics Office
NASA Ames Research Center
Moffett Field, CA, USA

Natasha Schatzman
Aerospace Engineer
Aeromechanics Office
NASA Ames Research Center
Moffett Field, CA, USA

ABSTRACT

Rotorcraft noise source identification is at the forefront of civil rotorcraft applications with the emergence of the Urban Air Mobility (UAM) market. Blade Vortex Interaction (BVI) has been identified as one key source of noise produced by a rotor. To predict BVI occurrences for various Urban Air Mobility (UAM) configurations, the RApid Blade and Blade-Vortex InTeraction (RABBIT) tool was developed and utilized. The tool is built from a Beddoes Wake Model, and computes variables such as miss distance and BVI angle to calculate an impulse factor, which is able to visualize BVI for a given vehicle and flight condition. A complete checkout of this tool and comparison with CAMRADII and ANOPP2/AARON, is performed. A wake comparison between RABBIT and CAMRADII is presented, and BVI is compared with ANOPP2/AARON's acoustic pressure time history to verify the tools effectiveness and accuracy. Three NASA Revolutionary Vertical Lift Technology (RVLT) concept vehicles were analyzed with increasing geometric and aerodynamic complexity, including the Quiet Single Main Rotor (QSMR), Side-by-Side, and Quadrotor. An analysis of the results concludes that RABBIT presents a low-fidelity tool that accurately predicts BVI location and intensity for multiple vehicle configurations and various flight conditions.

NOTATION

c	chord length (ft)
c_{l_α}	2D lift curve slope
C_T	coefficient of thrust $(\frac{T}{\rho A(\Omega R)^2})$
h	blade vortex miss distance (ft)
$\bar{I}$	impulse factor
R	rotor radius (ft)
r	spanwise radial position (ft)
r/R	dimensionless radial position
t	time (sec)
V_∞	downwash, induced inflow (ft/s)
V_{tip}	rotor blade speed (ft/s)
X	Cartesian coordinate, positive forward flight direction
Y	Cartesian coordinate, positive port direction
Z	Cartesian coordinate, up direction
α_{TPP}	shaft angle (degrees, positive nose up)
γ	Blade Vortex Interaction angle (deg)
Γ	nondimensional vortex strength $(\frac{\Gamma}{2\pi h V_b})$
$\Delta\psi$	wake age resolution (deg)
ψ_b	blade azimuth angle (deg)
λ_i	inflow (ft/s)
μ	average advance ratio
μ_x	advance ratio in the x direction
μ_z	advance ratio in the y direction
ρ	density of medium $(slugs/ft^3)$
Ω	rotor rotation rate (rpm)
$\frac{\partial F}{\partial t}$	time rate of change of loading

Presented at the VFS Aeromechanics for Advanced Vertical Flight Technical Meeting, San Jose, CA, Jan. 25–27, 2022.

INTRODUCTION

NASA's Revolutionary Vertical Lift Technology (RVLT) project emphasizes the importance of having versatile prediction tools to support the rotorcraft community. The tools are executed in a chain to predict primarily performance and acoustics of multirotor Vertical Take Off and Landing (VTOL) aircraft. Currently, the NASA RVLT toolchain has tools that predict and analyze rotorcraft acoustics, but these tools can be computationally expensive and time consuming and so a need exists for a rapid, lower fidelity acoustic prediction tool, particularly for use in the early stages of the design process. One such tool, the RApid Blade and Blade-Vortex InTeraction (RABBIT) tool was created to predict the location and description of Blade-Vortex Interaction (BVI) noise, which has been identified as one of the sources of rotorcraft noise that causes human annoyance (Ref. 1). RABBIT will enable engineers to quickly locate and understand designs or configurations that cause significant BVI noise.

Blade-Vortex Interaction is an aerodynamic condition

that occurs when the wake shed by the blade of a rotor interacts with another blade. This interaction causes an impulse in blade loading that creates both unsteady loading and a high-amplitude acoustic pressure signature (Ref. 2). As this resulting noise often causes annoyance in the community, finding ways to reduce BVI is an important area of study for both acoustics and aerodynamics.

To validate RABBIT, wake geometries were compared with the Comprehensive Analytical Model of Rotorcraft Aerodynamics and Dynamics II (CAMRADII) (Ref. 3) and BVI location predictions were compared with the Aircraft NOise Prediction Program 2 (ANOPP2) and the AeroAcoustic ROtor Noise (AARON) system (Ref. 4). Although ANOPP2 and AARON are noise prediction systems, the acoustic pressure time history can be used to identify BVI locations, which can be compared with the BVI outputs of RABBIT. CAMRADII and ANOPP2 calculations serve as validation for RABBIT.

RABBIT CAPABILITIES

Written in MATLAB, RABBIT was originally designed as a tool for coaxial rotors to identify the time and azimuth at which a reference blade of the upper (or lower) rotor crosses a lower (or upper) rotor blade to pinpoint locations of interest between or in the plane of the rotors (Ref. 1).

RABBIT has since been extended to become a more complete prediction tool. The tool is now capable of predicting BVI for various configurations such as single, coaxial, side-by-side, and quad rotors. Additionally, RABBIT was extended to read in CAMRADII wake data for BVI prediction to allow a user to use a higher fidelity wake to improve the accuracy of the BVI prediction. A GUI interface was also created to improve the user experience and clarify the required input.

There are several outputs that RABBIT is capable of producing. The first is a visualization of the wake procession overlaid with the blades of the rotor. Additionally, BVI impact points can allow the user to visualize BVI locations on the wake plot. Finally, RABBIT outputs the time rate of change of loading versus azimuth, which can give information on time and strength of BVI impact.

RABBIT also produces a video of the blades and their BVI passages, providing the user the ability to visualize the rotor and where BVI loading pulses are going to occur. This capability may help a user identify different flight conditions and rotor parameters that affect the magnitude of BVI noise produced.

RABBIT TECHNICAL BACKGROUND

RABBIT utilizes a Beddoes Wake Model to calculate the shed wake for every blade for a given temporal and azimuthal resolution. Impulse factor of a BVI occurrence is calculated for the wake provided by the Beddoes Wake Model. Initial validation of RABBIT was made with data published in Sim and George (Ref. 5).

Wake Model

RABBIT was designed as a tool for BVI prediction, and as such, utilizes lower fidelity calculation methods to improve computational speed compared to other codes such as CAMRADII. The wake model used in RABBIT is the Beddoes Wake Model (Ref. 6). This model is a prescribed wake model that uses generalizing assumptions to calculate tip vortex geometries. A free wake implementation, in comparison, tracks all wake geometries and uses them to calculate the inflow entering the rotor disk. RABBIT is not a general acoustic prediction tool, but instead utilizes vortex and wake parameters to visualize and predict only BVI noise.

To calculate the wake, RABBIT reads in a desired V_{tip}, α_{TPP}, μ and C_T and solves for Eqn.1. This momentum theory uniform inflow equation can be used to iteratively solve for inflow (λ_i) using a desired V_{tip}, α_{TPP}, μ and C_T, and then used to calculate the wake. RABBIT follows the same method and approach performed by Sim and George (Ref. 5).

$$\frac{C_T}{2\lambda_i} = \sqrt{(\mu_z + \lambda_i)^2 + \mu_x^2} \tag{1}$$

Equation 1 for λ_i can then be used to follow Beddoes method for calculating rotor downwash and vortex geometry. This method uses the location of the vortex in regards to the rotor disk to predict the effect of inflow on the vortex geometry. A full explanation of this method and how it is implemented can be found in Refs. 5 and 6.

As RABBIT uses a prescribed wake model, only a portion of geometric distortions caused by shed wake are considered when calculating both inflow and wake procession. The selected distortions are those in critical locations to the wake and all other locations are approximated (Ref. 6).

BVI Prediction

The method by Sim and George (Ref. 5) aimed to create a vortex-interaction calculation that modeled BVI blade loading efficiently and predicted noise directivity.

The wake that is released from the tip of the blade is used to predict a variety of important BVI parameters. Some of these include the BVI angle (γ), the vortex miss distance (h), the nondimensional vortex strength (Γ), and the time of impact (t). Two other relevant parameters are a BVI impulse factor ($\bar{I}$) and a time rate of change of loading ($\frac{\partial F}{\partial t}$) defined in Ref. 5.

$$\bar{I} = \frac{V_b cos\gamma}{h} \tag{2}$$

$$\frac{\partial F}{\partial t} = (c_{l_\alpha} c)(\frac{1}{2}\rho V_b^2)\bar{\Gamma}\bar{I}\frac{1-(\bar{I}t)^2}{(1+(\bar{I}t)^2)^2} \tag{3}$$

The impulse factor combines blade velocity (V_b), BVI angle (γ), and miss distance (h) into one definition for the location of the blade vortex. The time rate of change of loading combines the impulse factor ($\bar{I}$) with the vortex strength ($\bar{\Gamma}$) and

the loading of the blades to give a function that relates radiated acoustic pressure and time to the sources on the surface of the blade. Time rate of change of loading ($\frac{dF}{dt}$) can then be plotted versus azimuth to give a picture of BVI locations and their magnitudes.

Initial Validation

Using a simplified rotor, see Table 1, RABBIT is initially validated against Ref. 5. A comparison of the wakes from RABBIT and Ref. 5 is shown in Fig. 1 in the solid black (Beddoes) and red (RABBIT) line. Reference 5 also provided experimental, free and rigid wake calculations. Figure 1a shows identical procession of the wake in the z direction normalized over R between RABBIT and Ref. 5. The wake implementation also follows the general shape of both the free-wake and experimental wake.

Table 1. Simplified rotor specifications for validation from Sim and George.

Number of Blades	1
Blade Radius (R)	1.0 m
Chord Length	0.1 m
Angular Velocity (Ω)	1910 rpm
Forward Velocity (V_∞)	20 m/s
Coefficient of Thrust (C_T)	0.0050
Tip Path Plane Angle (α_{tpp})	2.9° (nose up)

Next, RABBIT's BVI location identification is compared to Sim and George in Fig. 1b. This plot shows locations where a BVI occurs for one blade over the course of one revolution. Differences are due to time step, wake time step, and tolerance of a BVI occurrences (distance from vortex to blade). The overall trend predicted by RABBIT matches well to the data provided by Sim and George.

The final comparison with Ref. 5 was for $\frac{dF}{dt}$ and is shown in Table 2. The simplified rotor was used and $\frac{dF}{dt}$ was calculated for five azimuth values. Both codes identified a maximum change in loading at 58° azimuth, and a close or exact match was found for all azimuth values except for 285°, where the difference was more pronounced.

Table 2. Comparison between RABBIT and Ref. 5 for normalized time rate change of loading ($\frac{dF}{dt}$).

ψ_b (deg)	Sim $\frac{dF}{dt}$	RABBIT $\frac{dF}{dt}$
30	0.07	0.07
58	1.00	1.00
81	0.20	0.15
285	-0.15	-0.45
315	-0.10	-0.11

Differences in value can be attributed to the difference in resolution, with Ref. 5 using a 2.5° temporal resolution and RABBIT using a 1° temporal resolution. Additionally, Ref. 5

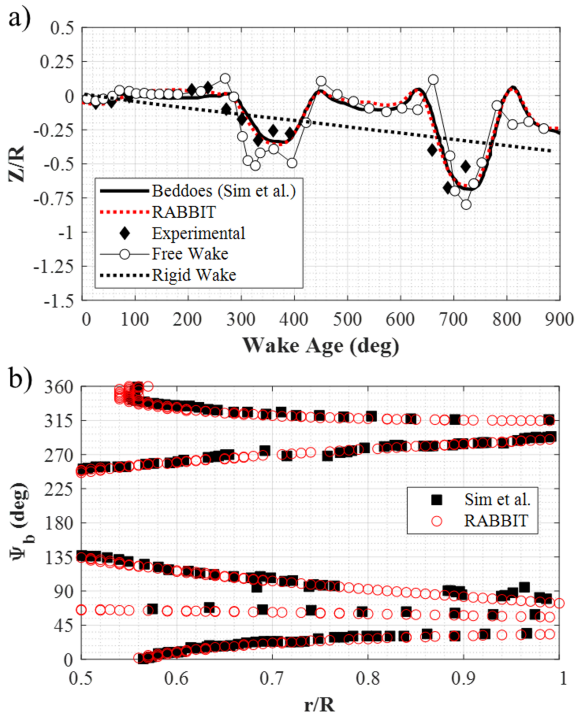

Figure 1. Comparison between RABBIT and Ref. 5 for a) wake geometry and b) BVI location.

does not provide values for BVI angle and other parameters, which prevents a more in-depth comparison. Generally, both Ref. 5 and RABBIT identify $\frac{dF}{dt}$ occurring at the selected azimuths, and only small differences in magnitude are present for some values.

Further validation of RABBIT was completed with CAMRADII and ANOPP2/AARON to provide a more complete analysis of the capabilities of RABBIT.

VALIDATION METHODS

RABBIT output is compared to results from CAMRADII (Ref. 3) and ANOPP2/AARON (Ref. 4) via the pyaaron script developed by Doug Boyd of NASA Langley (Ref. 7). The free wake computed by CAMRADII will be compared to the wake of RABBIT. BVI noise computed by ANOPP2/AARON and by RABBIT will be compared.

CAMRADII

CAMRADII, a comprehensive analysis code used by the NASA toolchain to calculate rotor dynamics and aerodynamics, was used to generate a wake that was compared with the wake computed by RABBIT (Ref. 3). CAMRADII has the option of using a a free wake model, which is higher fidelity than the Beddoes prescribed wake model used by RABBIT. A free-wake implementation accounts for all geometric distortions caused by shed wake when calculating both inflow and wake procession to get the most accurate wake procession

possible (Ref. 8). Beddoes's model shows good comparison against free wake models and is computationally less expensive.

The coordinate system in RABBIT and CAMRADII are opposite from each other, where CAMRADII X and Y results are negated and blade order is reversed in order to compare to RABBIT. Both codes were provided the same input when possible, with CAMRADII requiring additional information to model the complete aircraft. Modeling the whole vehicle in CAMRADII allows for the most accurate wake calculation, even though RABBIT only accounts for rotors.

ANOPP2/AARON

BVI comparisons were completed using the ANOPP2 and AARON system via pyaaron. pyaaron is a python program that runs CAMRADII, extracts the outputs, converts the CAMRADII outputs into inputs for ANOPP2 and AARON, and then runs ANOPP2 and AARON (Ref. 7). ANOPP2 utilizes Farassat's Formulation 1A of the Ffowcs Williams-Hawkings equation (Ref. 9) to perform acoustic calculations and has several output capabilities. While ANOPP2 is the framework that enables the acoustic calculations, AARON is a user code that accesses ANOPP2 functions for rotorcraft applications (Ref. 4).

The same coordinate axis is used for both RABBIT and ANOPP2/AARON. The positive axes are defined as the forward flight direction for X, port for Y, and up for Z. Additionally, to ensure that acoustic predictions are in the acoustic far-field, the distance of the observer will be a function of the rotor radius of each vehicle. The observer is placed at 10 rotor radii in front of the aircraft center (-X direction), 0 rotor radii away in the y direction, and 15 rotor radii under the aircraft (-Z direction), see Fig. 5 for origin and coordinate system reference.

ANOPP2/AARON's acoustic pressure time history output was selected as the method of visualizing BVI. BVI can be characterized in the acoustic time history by sharp positive pulse followed by a large negative sharp pulse (Ref. 2). With the exception of the initial vehicle analyzed, acoustic pressure time history results are not corrected for acoustic propagation time. This will cause an offset between RABBIT and ANOPP2/AARON results as RABBIT does not propagate to a microphone and therefore is not offset by time. This offset can be corrected by accounting for acoustic propagation time, which was completed for every analysis.

NASA REFERENCE VEHICLE SELECTION

To give a complete study of the implementation of RABBIT, three NASA urban air mobility (UAM) reference vehicles were studied and compared to RABBIT with analyses completed in CAMRADII and ANOPP2/AARON. Each NASA UAM reference vehicle has an increasingly complex rotor configuration including the QSMR (single rotor), Side-by-Side (two rotors), and Quadrotor (four rotors) (Ref. 10).

The QSMR is described in detail in Ref.10 and was selected because of its simple single-rotor configuration. This vehicle has the added feature of being designed for low noise, so it may be interesting when contrasted with other vehicles (Ref. 10). The baseline QSMR is a three-bladed six-passenger vehicle described in Table 3 and depicted in Fig. 2. For the QSMR, RABBIT ran for with a 1° timestep and output a wake for every 1°. A BVI has occurred if the distance between the blade and the vortex filament core is within a specified tolerance. For the QSMR, the tolerance was set to 5% of the blade chord.

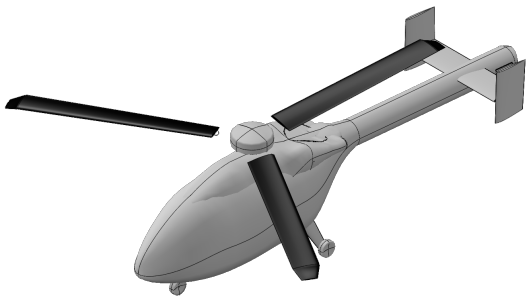

Figure 2. Three-Bladed QSMR vehicle depiction (modified vehicle from Ref. 10).

Table 3. QSMR specifications and flight condition.

Number of Rotors	1
Number of Blades	3
Rotor Radius, R (ft)	16.96
Chord Length (ft)	2.27
Blade phase (deg)	0, 120, 240
Tip Speed (ft/sec)	700
Advance Ratio, μ	0.12
Coefficient of Thrust, C_T	0.0015
Tip Path Plane Angle, α_{tpp} (deg)	-4 (nose down)
Microphone Location (x, y, z)	10R, 0R, -15R

The next vehicle considered was a UAM Reference Side-by-Side vehicle, depicted in Fig. 3 and described in Table 4 (Ref. 11). The Side-by-Side is a six-passenger vehicle with two counter-rotating rotors, each with 3 blades. The specific vehicle considered is a scale model of the Ref.11 Side-by-Side. The scale model was designed for wind tunnel testing (Ref. 12).

As this vehicle has two rotors, RABBIT must account for twice as many wakes. In RABBIT, each rotor only considers its own wake when calculating inflow, and the wakes do not interact. RABBIT does account for both wakes for BVI impacts on all blades. In this way, each blade is aware of all wakes produced by the vehicle. Both the time step and wake output in RABBIT were set to a resolution of 1°. Tolerance was set to 50% of the chord. This tolerance is larger than the

other vehicles as the flight condition selected doesn't have direct BVI impulses, but still a close enough vortex-passages to cause an acoustic reaction in the acoustic pressure plot. As BVI strength is caused by shed vortices, vehicles with high RPM can have a strong BVI response even when shed vortices don't directly impact the vehicle (Ref. 13).

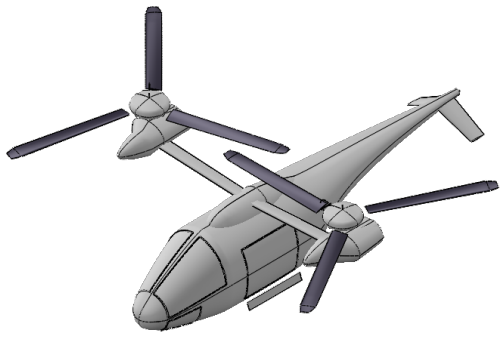

Figure 3. Side-by-Side vehicle depiction (modified vehicle from Ref. 11).

Table 4. Side-by-Side specifications and flight condition.

Number of Rotors	2
Number of Blades	3
Rotor Radius, R (ft)	1.34
Chord Length (ft)	0.10
Rotor Separation Distance	1.095R
Blade phase for rotor 1 (deg)	0, 120, 240
Blade phase for rotor 2 (deg)	60, 180, 300
Tip Speed (ft/sec)	350
Advance Ratio, μ	0.24
Coefficient of Thrust (per rotor), C_T	0.0057
Tip Path Plane Angle, α_{tpp} (deg)	-8 (nose down)
Microphone Location (x, y, z)	10R, 0, -15R

The final UAM reference vehicle analyzed using RABBIT was the quadrotor, depicted in Fig. 4 and described in Table 5 (Ref. 11). This four-rotor one-person vehicle is the most complicated vehicle modeled by the RABBIT tool. This vehicle contains four rotors arranged in an 'X' shape with the rear rotors elevated 0.35R above the front rotors. This vehicle requires RABBIT to account for the wakes of four separate rotors, and was considered to be an adequate final test of the capabilities of the RABBIT tool.

RABBIT wake and temporal resolution were set to 1°. Tolerance was set to 5% chord.

Specific flight conditions producing strong BVI for each vehicle were selected. For all vehicles, the flight conditions consist of a shallow descent angle with a nose-down configuration.

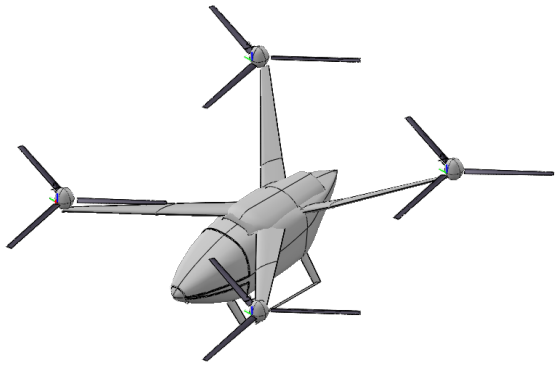

Figure 4. Quadrotor vehicle depiction (modified vehicle from Ref. 11).

Table 5. Quadrotor specifications and flight condition.

Number of Rotors	4
Number of Blades	3
Rotor Radius, R (ft)	9
Chord Length (ft)	0.75
Rotor Height Difference	0.35R
Blade phase, for all rotors (deg)	0, 120, 240
Tip Speed (ft/s)	550
Advance Ratio, μ	0.17
Coefficient of Thrust (front rotors, per rotor), C_T	0.0063
Coefficient of Thrust (rear rotors, per rotor), C_T	0.0058
Tip Path Plane Angle, α_{tpp} (deg)	-2.5 (nose down)
Microphone Location (x, y, z)	10R, 0, -15R

As each vehicle had different flight conditions, each was solved to have a different inflow value from Eqn. 1. Inflow values were iteratively solved given the flight parameters of that vehicle. Table 6 presents the values for each vehicle, and for both the front and rear rotors of the Quadrotor.

Table 6. RABBIT and CAMRADII inflow (λ_i).

Vehicle	CAMRADII	RABBIT
QSMR	0.0080	0.0063
Side-by-Side	0.0160, 0.0160	0.0119, 0.0119
Quadrotor front rotors	0.0198, 0.0198	0.0188, 0.0187
Quadrotor rear rotors	0.0200, 0.0199	0.0172, 0.0174

RESULTS

Completed analysis and discussions for the QSMR, Side-by-Side, and Quadrotor are presented. Three-dimensional wake geometries computed by RABBIT and CAMRADII are compared. BVI results are presented by comparing normalized time rate change of loading (dF/dt) with ANOPP2/AARON acoustic pressure time history. Physical explanations for results are discussed. Both RABBIT and CAMRADII were run

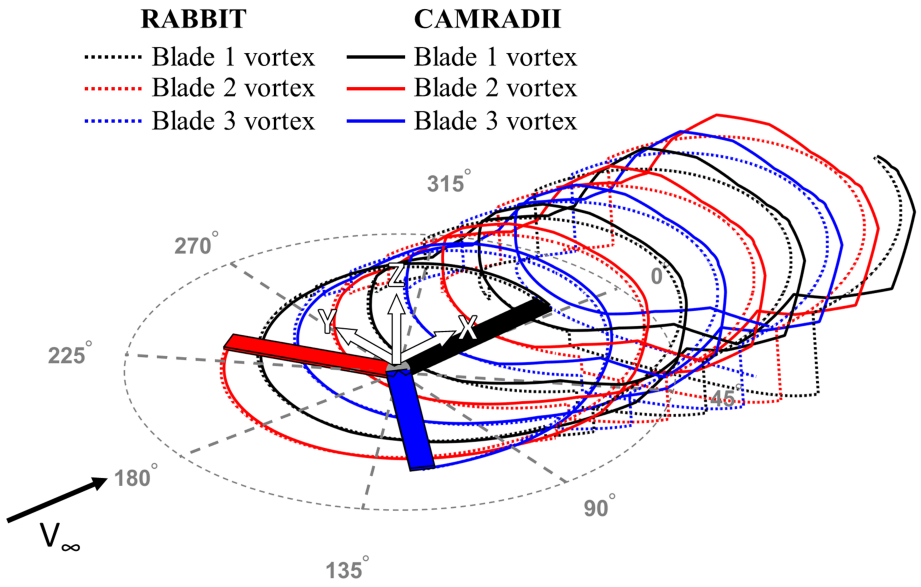

Figure 5. QSMR shed tip vortex comparison between RABBIT and CAMRADII for all blades (μ = 0.121, α_{TPP} = -4, and C_T = 0.0015).

at a time resolution of 1° and wake age of 1° per time step.

QSMR

The QSMR is a single-rotor with NOTAR configuration, and was selected for the initial comparison of RABBIT. To further simplify the initial comparison, only the main rotor was analyzed.

The wake geometry calculated by RABBIT was compared with the wake geometry calculated by CAMRADII. CAMRADII has several wake models of varying fidelity, ranging from a uniform inflow to a full free-wake implementation. For this study, RABBIT's wake was compared directly to the highest fidelity wake option of CAMRADII, the free-wake.

RABBIT and CAMRADII's wake is compared in Fig. 5, where RABBIT's wake is denoted by dotted lines and CAMRADII denoted by the solid lines. Each vortex is colored according to blade origin. CAMRADII results use a free wake with $\Delta\psi$ of 1° in post-trim, meaning that CAMRADII calculates a wake element for every 1° the rotor moves azimuthally. The post-trim analysis increases the resolution of the wake. RABBIT uses a prescribed wake with a $\Delta\psi$ of 1°.

Figure 5 highlights the limitations of a prescribed wake, as a prescribed wake loses accuracy as the wake convects away from the rotor. This is caused by a prescribed wake only accounting for vortex interactions near the rotor, with interactions being neglected as the rotor moves away. Figure 5 shows that RABBIT can accurately capture the mean movement of the wake, but cannot account for complex aerodynamic conditions. It is important to note that the benefit of RABBIT is not the wake accuracy, but the ease and speed of use and the clarity of results with respect to BVI.

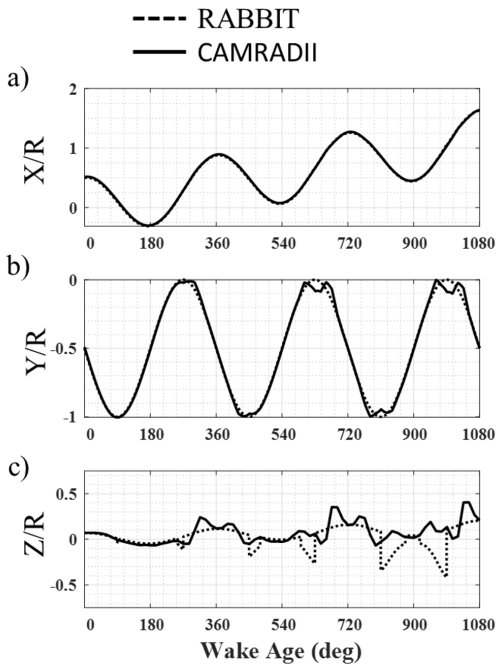

Figure 6. Tip vortex versus wake age comparison for the QSMR in RABBIT and CAMRADII for blade 1 at 0 degrees azimuth for a) X/R, b) Y/R, and c) Z/R (μ = 0.121, α_{TPP} = -4°, and C_T = 0.0015).

A wake comparison is further analyzed in Fig. 6 where the three-dimensional wake is separated into X/R, Y/R, and

Z/R as a function of wake age, where R is the radius. The comparison allows for a better understanding of RABBIT's strengths and weaknesses when modeling a rotor wake.

The accuracy in each direction is related to the wake of a previous time step and the effect of the wake on the inflow in that direction. There are minimal differences between the RABBIT and CAMRADII wakes in the X/R component. The wake in the Y and Z directions, on the other hand, is impacted by the re-ingestion of the wake by the rotor. This re-ingestion both alters the inflow of the rotor and the vortex being ingested. As a prescribed wake calculates mean inflow and does not have exact vortex tracking, any re-ingestion events will cause RABBIT and CAMRADII wakes to differ, as seen in Fig. 6.

Furthermore, the vortex filaments from each blade in RABBIT do not interact with each other, which further explains differences from the free wake calculation. Therefore, the Z direction is the least accurate match, as the Z direction is highly impacted by the rotor inflow lacking the inclusion of previous wake pulses.

Loading calculations from CAMRADII are analysed to highlight BVI locations on the blade. RABBIT BVI instances can be compared directly between CAMRADII loads and normalized $\frac{dF}{dt}$ calculated by RABBIT. The normal force (F_Z) for the QSMR is shown in Fig. 7, where BVI occurs on the advancing side of the rotor.

While F_Z in CAMRADII does not directly identify BVI, BVI is expected to occur on the advancing side of the rotor, so the blue loading changes in Fig. 7 are likely due to BVI. Additionally, differences between Fig. 7 and RABBIT's predictions may be due to the tolerance factor ignoring BVI that is considered less important due to the vortex's distance from the rotor disk, but still causing slight changes in loading.

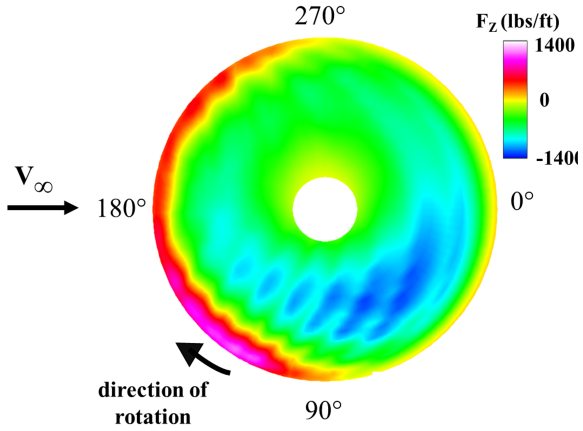

Figure 7. CAMRADII normal force (F_Z) calculations for the QSMR (μ = 0.121, α_{TPP} = -4°, and C_T = 0.0015).

The RABBIT computed wake procession for the QSMR main rotor is shown in Fig. 8 for every 0.33 revs (or 120° azimuth), for a tolerance factor of 5% of the chord. The tolerance factor in RABBIT determines when a BVI is considered based on the distance from the vortex core and blade. The BVI location visualized over time (Fig. 8) is one of the main deliverables of RABBIT and is similar to how loading on a blade can highlight BVI locations as shown in Fig. 7.

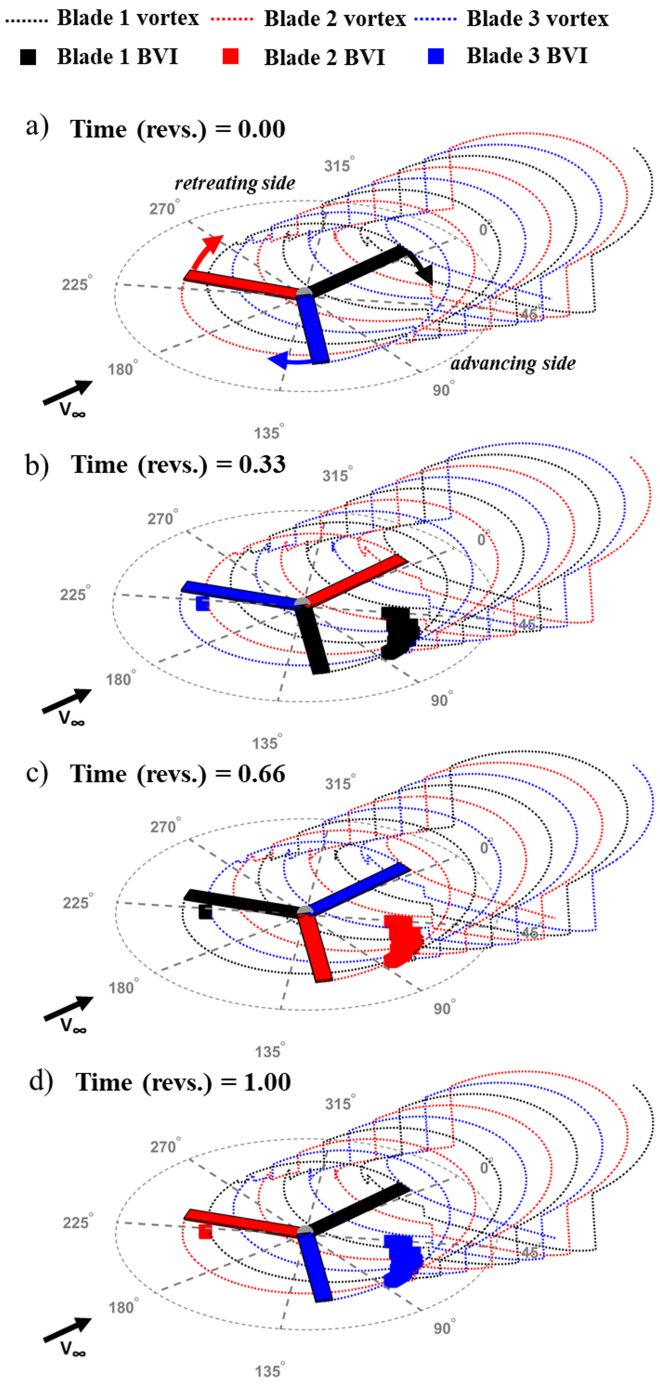

Figure 8. QSMR BVI location in RABBIT at a time (rev) of a) 0.00, b) 0.33, c) 0.66, and d) 1.00 (μ = 0.121, α_{TPP} = -4°, and C_T = 0.0015).

In Fig. 8, Blades 1, 2, and 3 are colored in black, red, and blue, respectively. The BVI occurrence is a colored square symbol with the same colorization of the blade that interacted

with the vortex. The total Fig. 8 shows one full revolution of the blade as it passes through the wakes of previous blade passages. As shown in Fig. 8b, the first blade (black) encounters several vortices around 90° and is flagged with a black square symbol. Next, the second blade (red) hits several vortices in the same location as the previous blade (90°) and is flagged with a red square symbol (Fig. 8c). And finally, the third blade (blue) hits several vortices again in the same location and is flagged with a blue square symbol (Fig. 8d).

As expected, BVI is occurring on the advancing side of the rotor, which is also shown in the CAMRADII load results in Fig. 7. This is caused by the high blade velocity on the advancing side of the rotor, where velocity of the blade is added to the velocity of the vehicle.

Both RABBIT and CAMRADII results show BVI occurrences around 90°, confirming validation of RABBIT's BVI location identification capability.

A comparison of normalized change in loading ($\frac{dF}{dt}$) output of RABBIT and CAMRADII as a function of one rotor revolution (not blade location) is shown in Fig. 9. Both the wake produced by RABBIT and the wake produced by CAMRADII were processed in RABBIT to calculate $\frac{dF}{dt}$ and were plotted together to compare results from the two wakes. As stated previously, $\frac{dF}{dt}$ combines blade velocity, BVI angle, miss distance, vortex strength, and blade loading to give a composite parameter of BVI. Both calculations were completed in RABBIT as CAMRADII does not calculate $\frac{dF}{dt}$ or some of the required parameters directly, so processing through RABBIT is required. As predicted in Fig. 8, there are three large BVI pulses per rotor period.

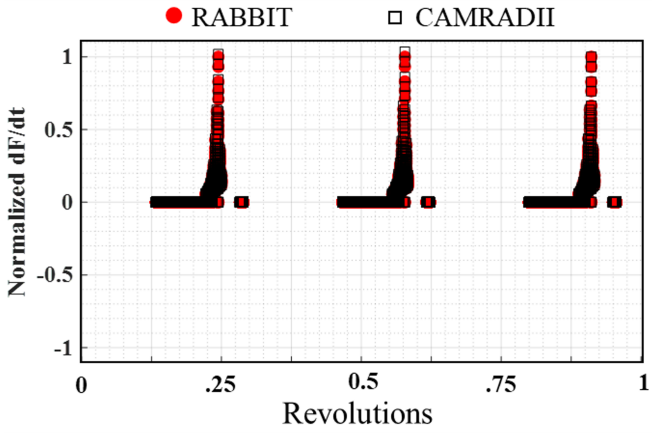

Figure 9. Normalized time rate change of loading for the QSMR with RABBIT wake and CAMRADII wake (μ = 0.121, α_{TPP} = -4°, and C_T = 0.0015).

Figure 9 shows that while CAMRADII and RABBIT have similar wakes, and therefore similar $\frac{dF}{dt}$'s, there are some small differences. The differences in magnitude and location are due to the the differences in the free wake and prescribed wake geometries. A general good match between the $\frac{dF}{dt}$'s of RABBIT and CAMRADII show the ability of RABBIT to accurately predict BVI location. Differences between Fig. 7 and Fig. 9 can be attributed to the tolerance factor in RABBIT ignoring weaker BVI, or other aerodynamic conditions affecting Fig. 7.

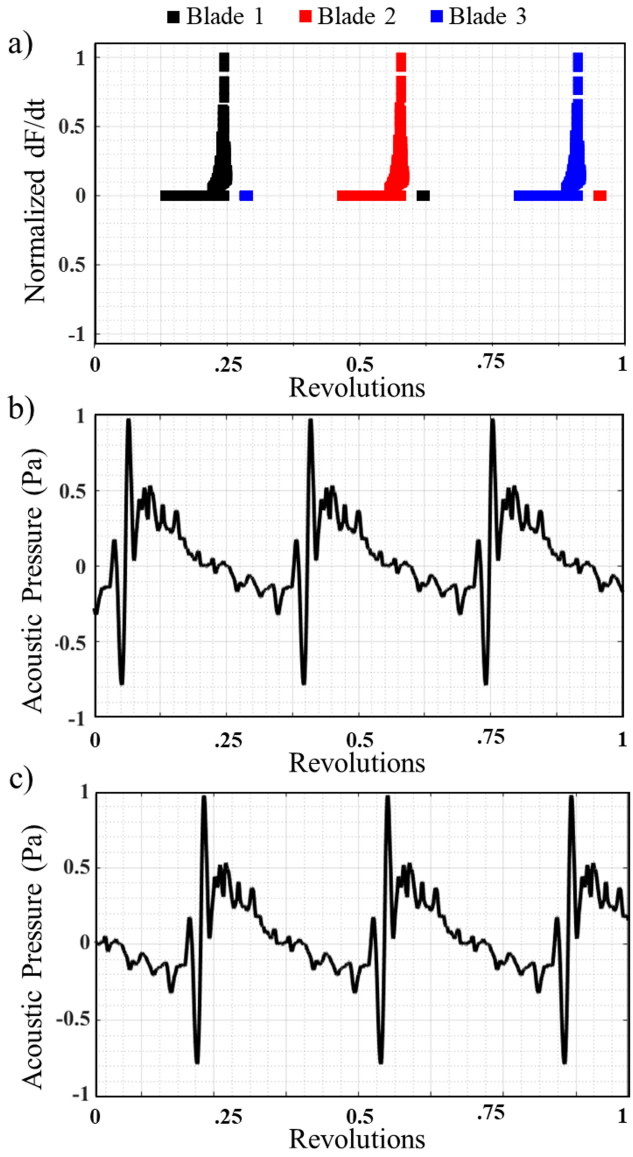

Figure 10. QSMR results for a) RABBIT normalized time rate change of loading, b) ANOPP2/AARON acoustic pressure for a microphone at (10R, 0, -15R), and c)ANOPP2/AARON acoustic pressure corrected for a propagation time of 0.27 sec (μ = 0.121, α_{TPP} = -4°, and C_T = 0.00149).

Finally, the analysis of the QSMR was completed with a comparison to ANOPP2/AARON. Figure 10 compares RABBIT with ANOPP2/AARON's acoustic prediction tools, namely acoustic pressure time history plotted for one rotor revolution. For the acoustic time history from ANOPP2/AARON, BVI noise is represented by a large pressure impulse for each blade when plotted over one period.

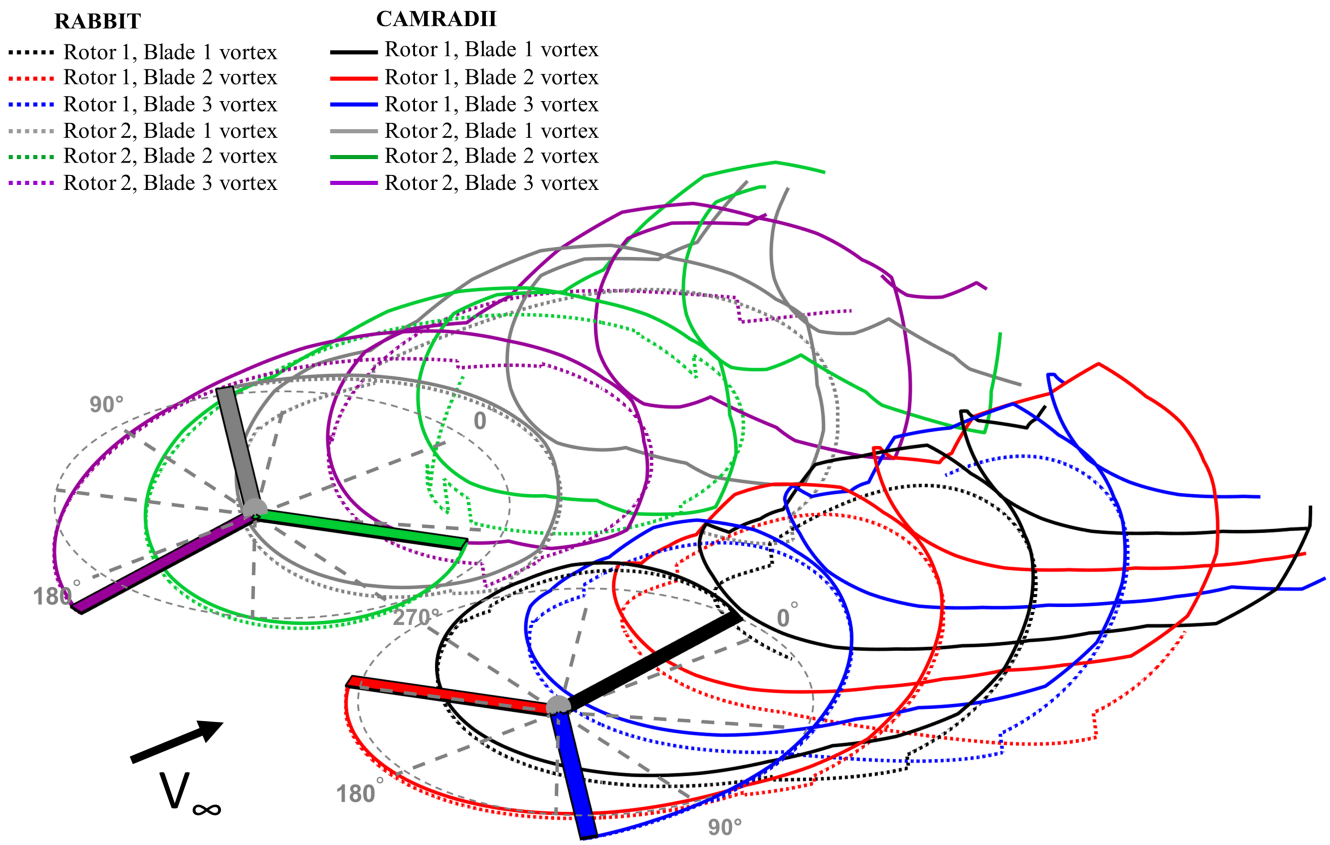

Figure 11. Side-by-Side shed tip vortex comparison between RABBIT and CAMRADII for all blades (μ = 0.239, α_{TPP} = -8°, and C_T = 0.0057).

In the case of the QSMR, BVI can be seen as three pressure spikes uniformly spread over the rotor period, shown in Fig. 10b.

Acoustic pressure time history is then directly compared to the the time rate of change of loading shown in Figure 10a. Time rate of change of loading captures a BVI pulse as it approaches a given blade location. A $\frac{dF}{dt}$ value of 1 corresponds to a close or exact blade-vortex intersection point that occurs nearly perpendicularly to the blade. Anything less than 1 indicates a vortex that is farther away or at an oblique angle from the blade but still causing a change in loading. This quantifies the strength of the BVI and how strong of a response it will cause. Figure 10 highlights how close time rate of change of loading can correspond to acoustic pressure, especially when propagation time is accounted for.

As $\frac{dF}{dt}$ is the mechanism that can quantify BVI intensity, a change in loading should occur at roughly the same azimuthal location as the acoustic pressure pulse and the highest changes in loading should correspond to the maximum acoustic pressures. The difference in azimuthal location corresponds to the location of the microphone and the time it takes for sound to propagate. For the case of the QSMR, the propagation time is 0.27 seconds, computed from the speed of sound of the atmosphere and the distance to the microphone. To compare the difference due to propagation time, direct ANOPP2/AARON results are shown in Fig. 10b and time corrected results are shown in Fig. 10c. All results going forward will be adjusted for propagation time directly.

Side-by-Side

As a continuation of the verification of RABBIT , the UAM Side-by-Side reference vehicle was analyzed. As this vehicle has two three-bladed rotors, the aerodynamic environment has twice as many rotors and wakes being produced that RABBIT must simulate.

A tip vortex trajectory comparison between RABBIT and CAMRADII is shown in Fig. 11, which highlights the limitations of the RABBIT prescribed wake compared to the CAMRADII free wake. As a reminder, RABBIT's use of a uniform inflow does not account for previous vortices impacting the inflow of current vortices, unlike CAMRADII. On the other hand, the Beddoes method has a similar, though less accurate, procession that leads to a more rapid prediction. The analysis of the Side-by-Side vehicle highlighted these differences and the impact they may have on the capabilities of RABBIT.

Results from RABBIT for the Side-by-Side are shown

in Fig. 12a (rotor 1) and Fig. 12b (rotor 2) for normalized $\frac{dF}{dt}$ over one revolution. Six sets of large magnitude BVI occurrences are shown. Since the rotors do not interact it is expected that rotor 1 and 2 will produce the same BVI locations and strengths but at a phase difference of 60° due to the starting position of each rotor.

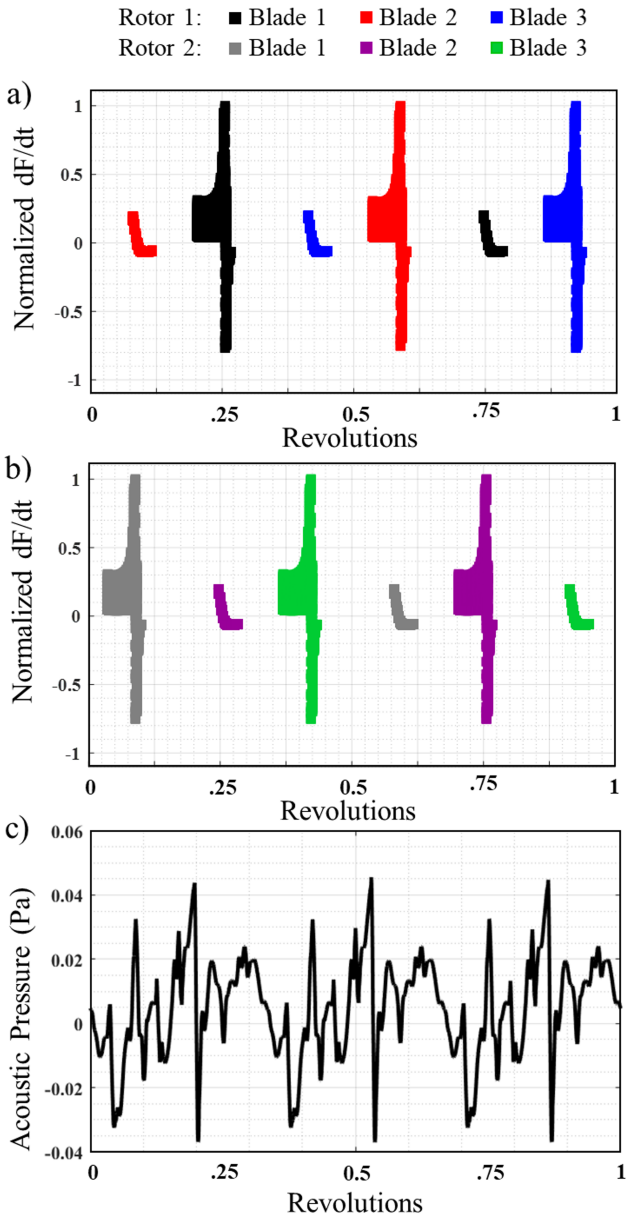

Figure 12. a) RABBIT normalized time rate change of loading for rotor 1, b) RABBIT normalized time rate change of loading for rotor 2, and c) ANOPP2/AARON acoustic pressure for a microphone at (10R, 0, -15R) shifted by 0.022 sec for the Side-by-Side (μ = 0.239, α_{TPP} = -8°, and C_T = 0.0057).

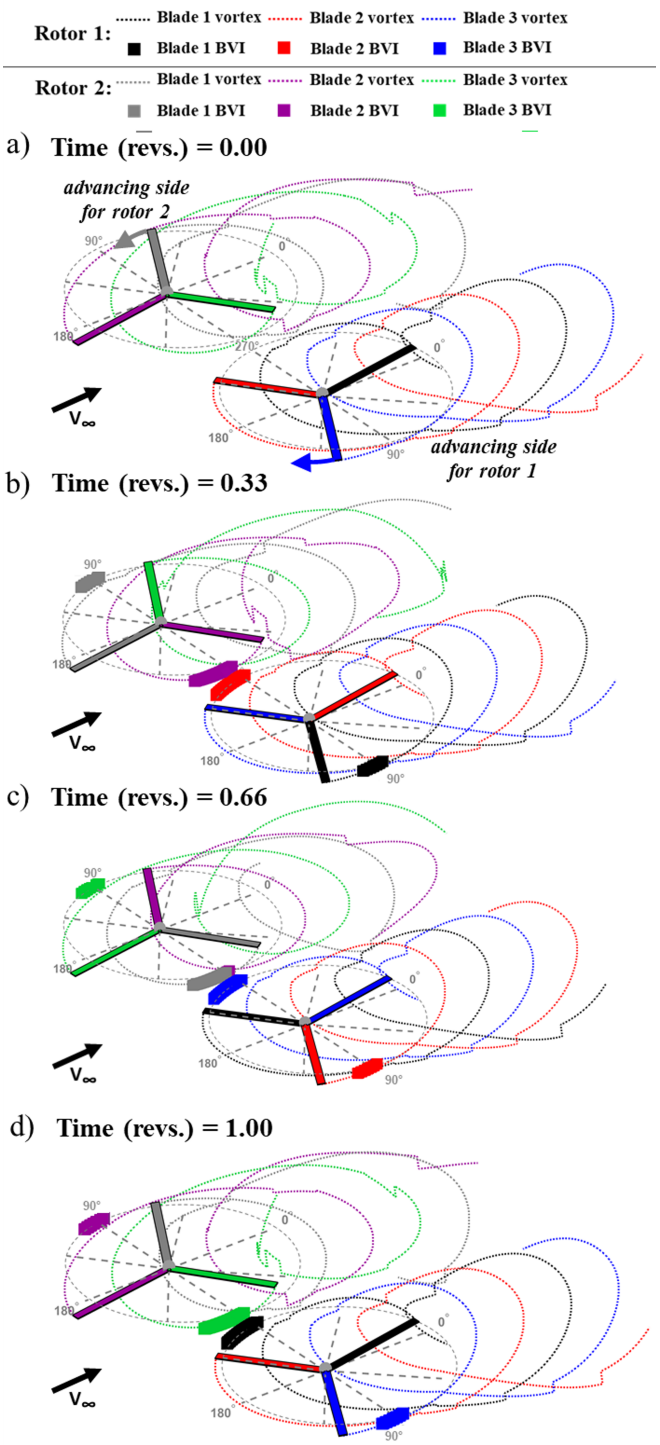

Figure 13. Side-by-Side BVI location in RABBIT at a time (rev) of a) 0.00, b) 0.33, c) 0.66, and d) 1.00 (μ = 0.239, α_{TPP} = -8°, and C_T = 0.0057).

When comparing RABBIT with ANOPP2/AARON results for the Side-by-Side, the benefit of having a tool for direct BVI prediction is evident. In Fig. 12c, six BVI pulses occur every 60°, similar to the RABBIT normalized $\frac{dF}{dt}$ showed in Fig. 12a and Fig. 12b. Though BVI is identified on the retreating as well as advancing side, the normalized time rate change of loading highlights that the BVI occurrence on the advancing side has a higher impulse factor compared to BVI from the retreating side, which cannot be ascertained from

Fig. 12c.

Figure 13 shows RABBIT wake procession for every one-third of a revolution (120°). BVI location is identified on both the advancing and retreating sides of the rotor and is highlighted in Fig. 13b when blade one on rotor one (black) rotates past 90° and blade one on rotor two (grey) rotates past 270° for the advancing side of each rotor. For Figs. 13c and d, the same BVI identification location occurs for the following blades on the advancing side.

When examining revolution 0.33 in Fig. 13b, four BVI occurrences can be seen, with one on the advancing side of each rotor (gray and black) and one on the retreating side of each rotor (purple and red). Figure 12a and Fig. 12b shows magnitude differences for BVI occurrences on the retreating side versus advancing side for each rotor. Retreating side occurrences are shown as smaller values of $\frac{dF}{dt}$ when compared with $\frac{dF}{dt}$ values on the advancing side. This can be shown within the first 0.1 rev where blade 1 of rotor 2 (gray) has a large $\frac{dF}{dt}$, while blade 2 of rotor 1 (red) has a smaller magnitude $\frac{dF}{dt}$. The noticeable difference between these rotors is that blade 1 of rotor 2 (gray) is on the advancing side, while blade 2 of rotor 1 (red) is on the retreating side. Similar analyses can be made for both Figs. 13c and 13d.

For the Side-by-Side, each blade passage comes in close contact with the wake of the other rotor, though RABBIT does not have the capability for the two wakes to interact, RABBIT can identify the BVI caused by this contact. This close passage further identifies why there are differences between the CAMRADII wake and RABBIT wake, previously seen in Fig. 11.

Quadrotor

The final simulation completed during the check-out of RABBIT was the Quadrotor. The Quadrotor is also a progression in complexity from the Side-by-Side, as the rear rotors interact with the wake from the front rotors and create a unique aerodynamic environment. RABBIT results for wake geometry and $\frac{dF}{dt}$ were computed and compared with both CAMRADII and ANOPP2/AARON to gain an understanding of RABBIT's capabilities and the BVI environment of the Quadrotor.

Figure 14 presents a comparison between the wake output from both CAMRADII and RABBIT for a single blade on each rotor. Figure 14a depicts CAMRADII's wake output, Fig. 14b depicts the RABBIT wake output, and Fig. 14c depicts the two wakes overlaid. The full RABBIT analysis was performed on all three blades for each rotor, but only a single vortex is shown for each rotor in Fig. 14 to reduce visual clutter. Rear rotors were offset vertically by 0.35R in both CAMRADII and RABBIT. The inflow on each rotor, especially in the case of the rear rotors, is highly altered by the wake of the other rotors. This leads to wakes that are highly distorted and less likely to be captured by anything less than a free-wake implementation. Currently the Quadrotor takes less than half the time to run with RABBIT compared to CAMRADII, but further optimizations are planned for RABBIT in the future, as the current run-time of two hours needs to be reduced.

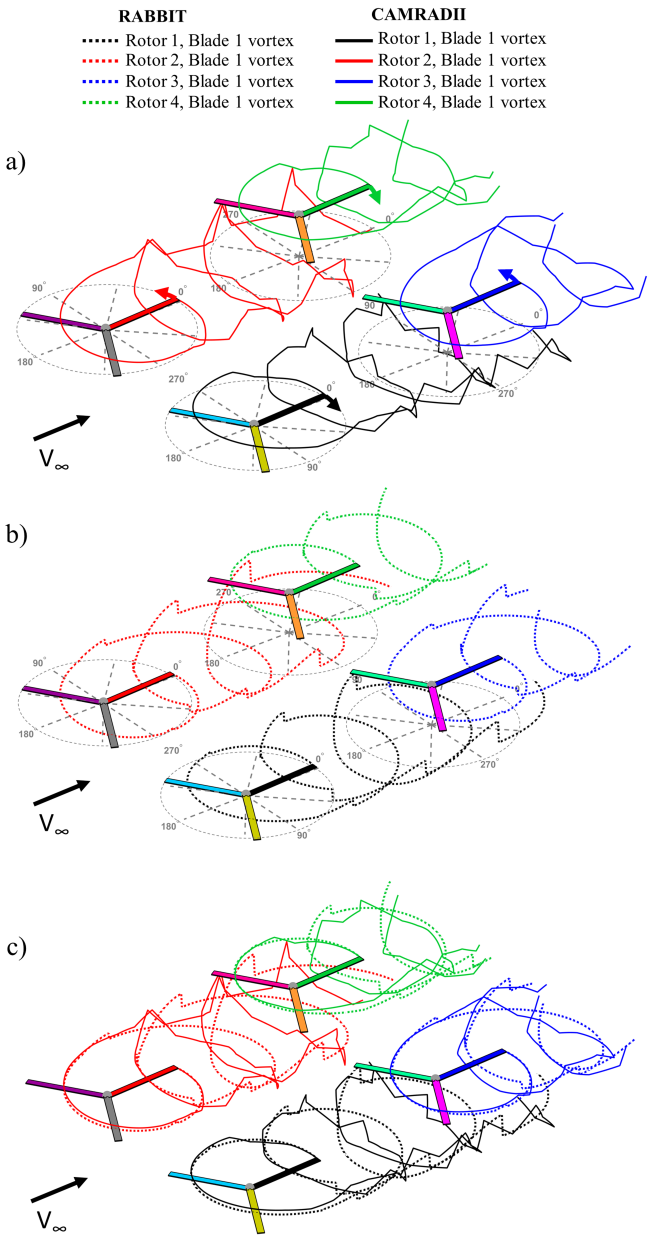

Figure 14. Quadrotor shed tip vortex comparison for one blade for a) CAMRADII, b) RABBIT, and c) CAMRADII and RABBIT (μ = 0.169, α_{TPP} = -2.49°, and C_T = 0.0063, 0.0063, 0.0058, 0.0058).

Figure 14 shows RABBIT maintaining accuracy for the first 270° of the shed wake, but as wake interactions become stronger, only the mean movement of the wake is captured. Discontinuities are seen as the wake is processed and re-ingested by the rotor, causing the large spikes seen by both implementations. Unlike RABBIT, CAMRADII propagates these interactions, causing the wakes to change drastically.

When BVI location is plotted over time, a more com-

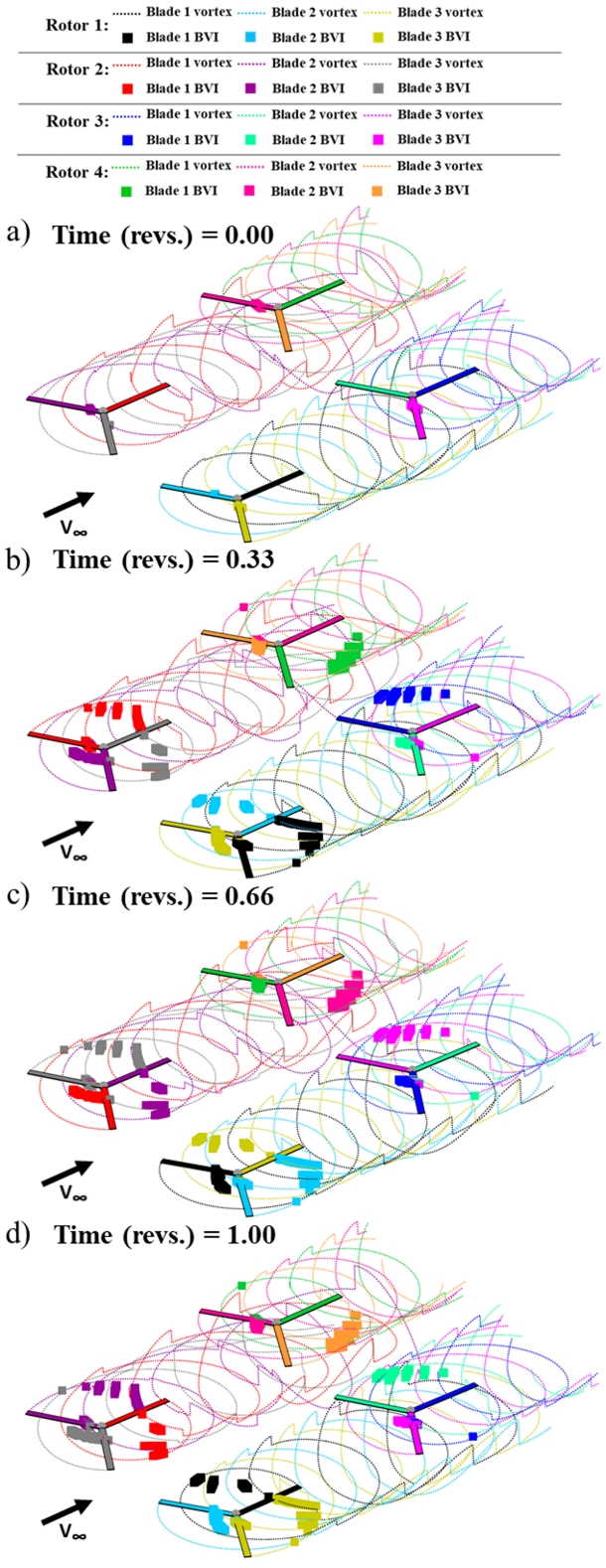

Figure 15. Quadrotor BVI location in RABBIT at a time (rev) of a) 0.33, b) 0.66, and c) 1.00 (μ = 0.169, α_{TPP} = -2.49°, and C_T = 0.0063, 0.0063, 0.0058, 0.0058).

plete picture of the interactions is revealed, as shown in Fig. 15. As seen for both the QSMR and Side-by-Side, the majority of high-amplitude BVIs occur primarily on the advancing side for each rotor and is further highlighted in the normalized $\frac{dF}{dt}$ as shown in Figs. 16a and 16b. As expected, a large portion of interactions occur on the rear rotors due to the wake from the front rotors, although the number of impacts is likely reduced by the vertical offset of the rear rotors. Regardless, the highest amplitude $\frac{dF}{dt}$s correspond to the advancing side of each rotor, with all other BVIs being lower in amplitude but more numerous in occurrence. This is likely due to the compact nature of the Quadrotor, but more analysis would be required to ascertain the reason for these low-amplitude impacts.

When compared with the previous two vehicles, the Quadrotor has by far the most BVI locations spread over the rotor disk. As all vehicles were operated at different flight conditions, the Quadrotor may be in a condition that exhibits more BVI than the other two. But, unlike the QSMR and Side-by-Side, this vehicle is subjected to more complex aerodynamic interactions due to the presence of four rotors, despite the front and rear rotors being vertically offset.

Finally, the change in loading for the Quadrotor was compared with the results for acoustic pressure developed in ANOPP2/AARON. The acoustic pressure time history for the Quadrotor presented in Fig. 16c represents the expected acoustic pressure for a vehicle with symmetry and rotors that rotate in opposite directions. That is, the three large spikes present in the pressure plots are caused by the six blades of the two front rotors. Due to these rotors being spaced the same distance from the microphone, and having the same but opposite phase, any acoustic propagation from them would impact the microphone at the same time, causing them to appear as one amplitude.

The three smaller pulses in the acoustic pressure time history plot are caused by the same conditions as the three main pulses, but these are due to contributions by the rear rotors. Once again, the rotors counter-rotating in the same phase result in three high-amplitude pulses, as both the left and right rotors contribute to the same pulse per blade. These pulses appear smaller in amplitude due to the rear rotors being farther away from the microphone, which was placed 10R in front of the center of the vehicle. The additional distance results in a smaller amplitude pulse.

Figures 16a and 16b show the normalized change in loading for the Quadrotor and ANOPP2/AARON acoustic time history predictions. Symmetry causes the rotors to be a mirror of each other, so they are shown in two figures to display all BVI points. Figure 16a depict the BVI points on the port rotors (rotors 1 and 3). Figure 16b represent starboard rotors (rotors 2 and 4). These plots show what was predicted in Fig. 15, that the majority of BVI impacts are on the rear rotors, but there is still a significant pulse as a function of blade passage for each front rotor. Additionally, there are BVI occurrences along the entire period contributed from the front rotors.

Further analysis of the Quadrotor results should be performed to clearly identify each contributing BVI occurrence.

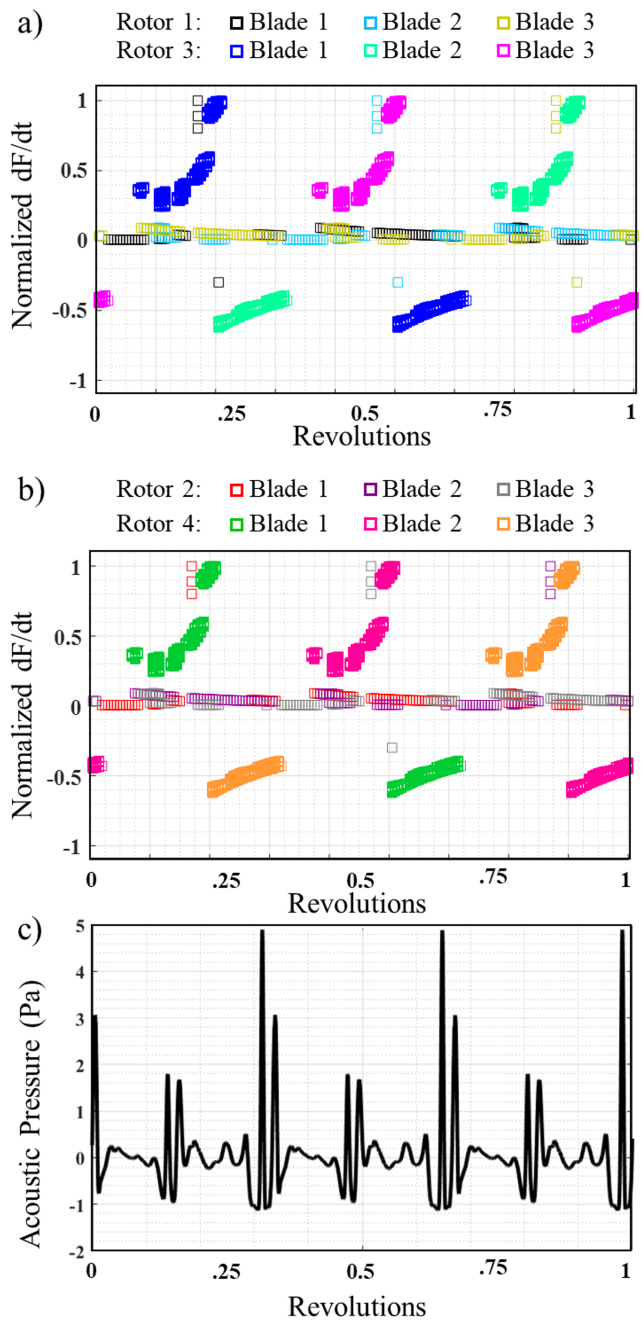

Figure 16. a) RABBIT normalized time rate change of loading for Rotors 1 and 3; b) RABBIT normalized time rate change of loading for Rotors 2 and 4; and c) ANOPP2/AARON acoustic pressure for a microphone at (10R, 0, -15R) shifted by 0.143 sec (μ = 0.169, α_{TPP} = -2.49°, and C_T = 0.0063, 0.0063 0.0058, 0.0058).

To perform this study, contributions of each isolated rotor as well as a rotor-by-rotor build up of the Quadrotor should be considered.

CONCLUDING REMARKS

The RABBIT tool for BVI prediction was introduced. Output capabilities were presented, and the internal model was verified via comparison with two other established tools.

Three NASA reference vehicles were used to demonstrate the capabilities of RABBIT including the Quiet Single Main rotor, Side-by-Side, and Quadrotor. Each vehicle was first modeled with CAMRADII to see the differences between the prescribed wake used in RABBIT with the free-wake used in CAMRADII. BVI comparisons were made with ANOPP2/AARON to compare the BVI locations and amplitudes with traditional acoustic prediction methods, namely acoustic pressure time history.

The QSMR RABBIT results identified three strong BVI pulses as also shown in the ANOPP2/AARON results, as expected of a three-bladed rotor. Side-by-Side RABBIT results predicted six BVI pulses, three strong and three weaker. This was once again reflected by the ANOPP2/AARON results and that the vehicle has six blades. Finally, the Quadrotor predicted six BVI pulses, three strong and three weak, which is caused by the 12-bladed vehicle having symmetry and rotors with the same period. ANOPP2/AARON also validated these results. All three vehicles had RABBIT results that compared well with CAMRADII and ANOPP2/AARON.

Although results matched, limitations of RABBIT were also found. Wake limitations when compared to a free wake for vehicles with multiple rotors were discovered. Additionally, computational time increased with vehicle complexity, and may require addressing for future implementations.

RABBIT is shown to be a useful BVI prediction tool capable of visualizing BVI as a function of various parameters. Impulse factor and time rate of change of loading allows for a unique BVI prediction technique that provides information on impulse strength, location, and frequency.

ACKNOWLEDGMENTS

The authors would like to thank Lillian Tso for her contributions to algorithm improvements within MATLAB and GUI development of RABBIT. Special thanks to Wayne Johnson, Chris Silva, and Doug Boyd for their assistance with the toolchain and technical guidance while writing this paper. Thanks also to Bill Warmbrodt, Gloria Yamauchi, and Ethan Romander for their support on writing this paper and their general mentorship.

REFERENCES

1. Schatzman, N. L., "Aerodynamics and Aeroacoustic Sources of a Coaxial Rotor," NASA TM 219895, April 2018.

2. Schmitz, F. H. and Boxwell, D. A., "In-Flight Far Field Measurement of Helicopter Impulsive Noise," American Helicopter Society 32nd Annual Forum, Washington, D. C., May 1976.

3. Johnson, W., "CAMRAD II Comprehensive Analytical Model of Rotorcraft Aerodynamics and Dynamics," Johnson Aeronautics, Palo Alto, CA, 2005.

4. Lopes, L. V., Burley, C. L., "Design of the Next Generation Aircraft Noise Prediction Program: ANOPP2," 17th AIAA/CEAS Aeroacoustics Conference Proceedings, Portland, OR, June 2011. DOI: 10.2514/6.2011-2854.

5. Sim, B. W., George, A. R., "Development of a Rotor Aerodynamic Load Prediction Scheme for Blade-Vortex Interaction Noise Study," American Helicopter Society 51st Annual Forum, Fort Worth, TX, March 1995.

6. Beddoes, T. S., "A Wake Model for High Resolution Airloads," Proceedings of the 2nd International Conference on Basic Rotorcraft Research, Univ. of Maryland, College Park, MD, 1985.

7. Silva, C. and Johnson, W., "Practical Conceptual Design of Quieter Urban VTOL Aircraft," Vertical Flight Society's 77th Annual Forum and Technology Display, Virtual, April 2021.

8. Johnson, W., "A General Free Wake Geometry Calculation For Wings and Rotors," American Helicopter Society 51st Annual Forum, Fort Worth, TX, May 1995.

9. Farassat, F., "A Review of Propeller Discrete Frequency Noise Prediction Technology with Emphasis on Two Current Methods for Time Domain Calculations," *Journal of Sound and Vibration*, Vol. 71, (3), Aug. 1980, pp. 399–419. DOI: 10.1016/0022-460X(80)90422-8.

10. Johnson, W., "A Quiet Helicopter for Air Taxi Operations," Vertical Flight Society Aeromechanics for Advanced Vertical Flight Technical Meeting, San Jose, CA, January 2020.

11. Johnson, W., Silva, C., and Solis, E., "Concept Vehicles for VTOL Air Taxi Operations," American Helicopter Society Specialists' Conference on Aeromechanics Design for Transformative Vertical Flight, San Fransisco, CA, January 2018.

12. Wright, S. J. and Cummings, H., "Pre-test Comprehensive Analysis for the Urban Air Mobility Side-by-Side Test Stand", Vertical Flight Society Specialists' Conference on Aeromechanics Design for Transformative Vertical Flight, San Jose, CA, January 2021.

13. Schmitz, F., and Sim, B. W., "Radiation and Directionality Characteristics of Advancing Side Blade-Vortex Interaction (BVI) Noise," 6th AIAA/ CEAS Aeroacoustics Conference, Lahaina, HI, June 2000. DOI: 10.2514/6.2000-1922.